



Fano-Lorentz shape controlled by the collective effect of the nuclear ensembleTian-Jun Li ¹, Xin-Chao Huang,^{2,*} Zi-Ru Ma,¹ Bo Li,¹ Xi-Yuan Wang,¹ and Lin-Fan Zhu ^{1,†}¹*Hefei National Research Center for Physical Sciences at the Microscale and Department of Modern Physics, University of Science and Technology of China, Hefei, Anhui 230026, People's Republic of China*²*European XFEL, Holzkoppel 4, 22869 Schenefeld, Germany*

(Received 30 September 2022; revised 25 August 2023; accepted 12 September 2023; published 26 September 2023)

The thin-film planar cavity implanted in the Mössbauer nuclei has been developed as a powerful platform to study the light-matter interaction in the x-ray band. Herein the asymmetric and symmetric profiles of Fano interference are studied by controlling the collective effect and modifying the cavity structure. It is found that the asymmetric profiles in the overcritical and undercritical regimes are the Fano-Lorentz shape, and the asymmetry of the profile is determined by $\cos\varphi$ rather than $\cot\varphi$ in the framework of the initial Fano theory with φ being the phase shift of the continuum. In addition, the Fano-Lorentz profile not only can be controlled by the phase difference of the two pathways, but also can be adjusted by the weight of the normal Fano resonance in the Fano-Lorentz profile through regulating the collective effect of the nuclear ensemble. By varying the nuclear abundance at the cavity mode angle, the transformation between the symmetric peak and valley is observed in the overcritical regime, whereas the symmetric peaks are always presented in the undercritical regime. Furthermore, a particularly interesting phenomenon of a flat reflectivity, as if the resonant nuclear ensemble is not excited, is predicted in the nuclear ensemble at a critical nuclear abundance in the overcritical regime. The present results will not only confirm the presence of the complex q , but also open up an avenue to study the decoherence processes via the Fano-Lorentz shape in the thin-film planar cavity.

DOI: [10.1103/PhysRevA.108.033715](https://doi.org/10.1103/PhysRevA.108.033715)**I. INTRODUCTION**

An ensemble of N static atoms can be excited into an entangled state by the photon field, resulting in some intriguing effects caused by the resonant dipole-dipole interaction (RDDI), such as directed spontaneous emission [1,2], subradiance [3,4], as well as the collective Lamb shift (CLS) [5–7] that arises from the surreal virtual process within the atomic ensemble. Distinguished by the characteristic spatial phase $e^{i\mathbf{k}\cdot\mathbf{r}_j}$, the entanglement of the atomic ensemble can be classified into the symmetric Dicke state and the timed Dicke state according to different wavelength limits, where \mathbf{r}_j represents the position of the j th atom [5]. For the timed Dicke state, the RDDI can be precisely controlled by the position of the emitters, but the number of emitters is of course extremely limited [7,8], i.e., the timed Dicke state is not suitable for the strong collective effect. In order to exhibit the strong collective effect, the symmetric Dicke state requires a longer wavelength than the interatomic distance, such that each individual atom can be approximately regarded as identical and the number of atoms can be greatly increased consequently by the nanometer-thick atomic layer [6,9].

Except for the unique phenomena, the collective effect of the atomic ensemble is also expected, because the enhancement factor \sqrt{N} is important in various systems [10–14]. Benefitting from the enhancement of the collective effect,

Rabi oscillation has been observed in the Rydberg atoms bypassing the strong-coupling regime [15]. Additionally, the enhancement can also speed up the spontaneous radiation, resulting in the so-called superradiance (SR) that has been observed widely in lots of subfields of physics including astrophysics [16], cavity QED [9,17–19], quantum dots [20], Paul trap [8], as well as Bose-Einstein condensates [21].

Over the past decade, x-ray quantum optics has thrived with the development of high-brilliance synchrotron radiation and the x-ray free electron laser (XFEL) [22–24]. Designed with several nanometer-scale thickness layers and probed in the milliradian grazing incidence as sketched in Fig. 1(a), the thin-film planar cavity becomes one promising platform to study the x-ray photons-matter interaction and opens an avenue for x-ray quantum optics. Due to the small incident angle, the field wavelength of the standing wave in the z axis is significantly expanded, thus the effective symmetric Dicke state can also be realized in the x-ray cavity, albeit the short x-ray wavelength [9]. In addition, utilizing this artificial system, a set of fundamental phenomena have been studied such as CLS [9,25], electromagnetically induced transparency [26,27], spontaneously generated coherence [28], and Rabi oscillations [29], as well as controlling the core-hole lifetime [30], to name a few. In theory, Parratt formalism [31] and layer formalism [32] have been used as benchmarks for modeling the experimental results. In addition, the phenomenological few-mode model [33,34], Green function [35], as well as the *ab initio* quantum model [36] were also developed in parallel to gain a deep understanding of the mechanism.

*xinchao.huang@xfel.eu

†lfzhu@ustc.edu.cn

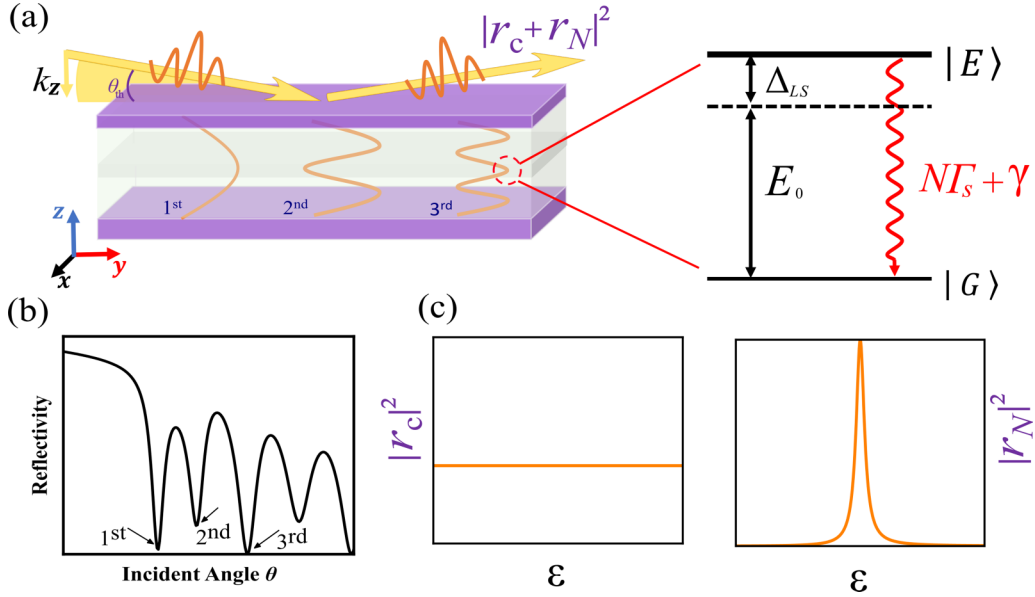


FIG. 1. The schematic design of the thin-film planar cavity. (a) The ensemble of the isotope (^{57}Fe marked as the gray layer) is in the center of the transparent guiding layer with the low-density material C. The cladding layers (purple) act as mirrors with the same high-electron-density materials; for example, Pt is used for the overcritical regime and Pd is used for the undercritical regime in this work. Excited by the cavity mode, the symmetric Dicke state of the nuclear ensemble has cavity-induced CLS and SR. (b) The reflectivity of the bare cavity with some notable dips that represent the excited cavity modes. (c) At the energy scale of SR, the reflectivity of the bare cavity (r_c) can be regarded as the continuum, while the reflectivity of the nuclear ensemble (r_N) is the discrete state.

In this work, the collective effect is employed to control the Fano interference, which is investigated via intercalating resonant Mössbauer nuclei (^{57}Fe) with various nuclear abundance in the thin-film planar cavity. Calculated by the benchmark CONUSS package [37,38], the asymmetric profiles of the Fano interference show inconsistency with the phase shift of the two pathways in the framework of the real parameter q . By introducing the complex q , this inconsistency can be explained by treating the asymmetric profiles in the overcritical and undercritical regimes as the Fano-Lorentz type viz. the incoherent superposition between the normal Fano resonance and a Lorentz peak. In the framework of the Fano-Lorentz profile, the weight and its range of normal Fano resonance are related to the collective effect of the nuclear ensemble and cavity regime, respectively. By adjusting the nuclear abundance, the undercritical cavity always has the symmetric peak at the cavity mode angle, while the transformation among the symmetric peak, flat line, and valley is observed in the overcritical cavity. As for the flat line, it corresponds to a critical nuclear abundance where the resonant nuclear ensemble seems to be “unexcited” superficially. From the viewpoint of destructive interference, this interesting phenomenon is explained self-consistently by the controllable relative amplitude of the two pathways [39].

II. MODEL

Containing different multilayer stacks of dielectric media, the thin-film planar cavity is sketched simply in Fig. 1(a). The ensemble of resonant Mössbauer nuclei is represented by the gray layer and sandwiched between the transparent guiding layers with low-density material. Cladding the purple layers with the high-electron-density materials and thin thickness,

the external x-ray field can be coupled into the cavity evanescently [40], and the reflectivity presents some notable dips correspondingly at some grazing incident angles, as shown in Fig. 1(b). As mentioned above, there are several methods to study the properties of the thin-film planar cavity, such as Parratt formalism [31] and the phenomenological few-mode model [33,34]. Parratt formalism is convenient to calculate the reflectivity of the multilayer system, but it cannot give an analytic expression to understand the reflectivity behavior deeply. As for the phenomenological few-mode model [33,34], although it is not an *ab initio* method, it can explain the reflectivity conveniently with the fitted cavity parameters such as the coupling strength κ_R and cavity decay rate κ . It should be noted that it is difficult to give a direct connection between the cavity parameters in the phenomenological few-mode model and the actual cavity parameters such as layer thickness, because there is not an analytic expression for the total reflectivity of a multilayer film by Parratt formalism. In order to study the thin-film planar cavity deeply, the phenomenological few-mode model is used in this work.

When the thin resonant layer is implanted at the antinode of the cavity mode, according to the phenomenological few-mode model, the nuclear ensemble can be excited to the collective state

$$|E\rangle = \frac{1}{\sqrt{N}} \sum_{n=1}^N |\downarrow_1 \cdots \uparrow_j \cdots \downarrow_N\rangle, \quad (1)$$

where \downarrow_j and \uparrow_j are the ground and excited states of the j th nucleus. For such a system, the total reflectivity is the coherent superposition of two pathways, where r_N is the contribution from the nuclear ensemble and r_c is from the bare cavity without the resonant Mössbauer nuclei, and the spectral

observation in reflectivity can be written by a general expression [34,41]

$$|R|^2 = \left| r_c |e^{i\varphi} + \frac{cN\Gamma_s/2}{\Delta - \Delta_{LS} + \frac{i}{2}(N\Gamma_s + \gamma)} \right|^2. \quad (2)$$

Here, $|r_c|$ is the magnitude of the bare cavity and φ is the phase difference of the two pathways. c is the amplitude of the discrete state. $\Delta = E - E_0$ is the energy detuning between the external x-ray field E and the nuclear excited transition energy E_0 . Δ_{LS} is the cavity-induced CLS, and the spontaneous radiation γ (4.7 neV) is broadened by $N\Gamma_s$ with the single-atom broadening width Γ_s and the nuclear number N . In the cavity, due to the one-dimensional (1D)-standing waves driven by the x-ray field, the number of the nuclei N is actually the one-dimensional effective nuclear number N/A (area density of the layer) [35,36] given by

$$\frac{N}{A} = d\rho_V f_{LM} a \quad (3)$$

Herein, A is the parallel quantization area. ρ_V is the density of the Mössbauer nuclei, f_{LM} is the Lamb-Mössbauer factor, and d and a are the thickness and abundance of the resonant layer, respectively [41].

Depending on the coupling strength κ_R of the external x-ray field with the cavity mode, cavity decay rate κ , and cavity detuning Δ_c , the bare cavity fulfills $r_c = 2\kappa_R/(\kappa + i\Delta_c) - 1$ in the phenomenological few-mode model [33,34], where the cavity detuning Δ_c reads

$$\Delta_c = \left(\frac{\sin \theta_{th}}{\sin \theta} - 1 \right) E_0. \quad (4)$$

Here, θ_{th} is the angle of the cavity mode and θ is the grazing incident angle. In detail, the bare cavity has a large linewidth (~ 100 eV) owing to the low Q , which is far wider than the broadened resonant width ($\sim \mu\text{eV}$) [9]. In detail, $\kappa > \kappa_R$ is always present in the thin-film planar cavity due to incoherent scattering and coupling between the cavity field and the outgoing modes [33]. Correspondingly, given by $c = 2\kappa_R/\kappa$, the amplitude of the discrete state is relevant to cavity property. Hence, $c = 1$ is the critical coupling condition and $1 < c < 2$ ($0 < c < 1$) represents the overcritical (undercritical) regime [33,34,42], which is similar to the magnon-photon system [43].

Owing to the remarkably different linewidth, the reflectivities from the bare cavity and nuclear resonance can be regarded as the continuum and the discrete state, respectively. As shown in Fig. 1(c), the interference between the continuum and discrete state results in Fano resonance. Described by the famous asymmetric parameter q , Fano resonance has been studied widely in lots of fields [44–52]. Fulfilled $q = \cot\varphi$ quantitatively [53–55], the asymmetric parameter q depends on the phase shift φ of the continuum, i.e., the profile of the Fano resonance arises from the phase shift of the two pathways essentially. For $\varphi \rightarrow n\pi$ (n is an integer), $q \rightarrow \pm\infty$, the Fano resonance will show the Lorentz shape. For $\varphi \rightarrow (n + 1/2)\pi$, $q \rightarrow 0$, the Fano resonance will show the symmetric “window resonance.” In general, the asymmetric profile shows the right peak for the positive q and the left peak for the negative q .

As for the collective effect of the nuclear ensemble, it can be seen from Eq. (3) that the enhancement of collective effect can be adjusted by the thickness or the abundance of the resonant layer. However, for the different thickness of the resonant layer the property of the cavity will be changed concomitantly. Hence, the abundance of Mössbauer nuclei is considered naturally, i.e., the weight of nuclear resonance process in the resonant layer is changed by the nuclear abundance without changing the absorption from electrons. Compared to the electronic transition [30], changeable abundance of the Mössbauer nuclei is also one of the advantages to the x-ray quantum optics.

III. RESULTS AND DISCUSSION

A. Fano resonance with a complex q

In order to study the Fano resonance comprehensively, different cavity regimes are designed in this work. The overcritical, undercritical, and critical cavity structures are Pt (0.5 nm) /C (20.8 nm) /⁵⁶Fe (0.6 nm) /C (19.6 nm) /Pt (2.5 nm), Pd (3.5 nm) /C (20.8 nm) /⁵⁶Fe (0.6 nm) /C (19.6 nm) /Pd (2.5 nm), and Pd (4 nm) /C (18 nm) /⁵⁶Fe (1.2 nm) /C (18 nm) /Pd (14 nm), respectively. As mentioned above, the asymmetric profile of Fano resonance depends on the phase shift φ of the continuum. Through calculating the reflectivities and fitting them with the phenomenological few-mode model, the parameters in the phenomenological few-mode model are obtained. The fitted process and cavity parameters are shown in the Appendix, and the fitted results are shown in Fig. 2(a). Given by $\varphi = \arg(2\kappa_R - \kappa - i\Delta_c) + \arg(\kappa + i\Delta_c) + \pi/2$, the phase shifts φ of the continuum versus the cavity detuning Δ_c are calculated and shown in Fig. 2(b). From Fig. 2(b), it can be seen that the phase shift of the Fano interference in the thin-film planar cavity can be understood in three cases:

(i) When the incident angle is smaller than the mode angle ($\theta < \theta_{th}$), the phase shifts in the overcritical and critical regimes are in the range $(0, \frac{\pi}{2})$, while it is in the range $(-\frac{\pi}{2}, \frac{\pi}{2})$ in the undercritical regime. In the framework of the initial Fano theory, there are positive q for the former, while there are both positive and negative q for the latter.

(ii) When the incident angle is larger than the mode angle ($\theta > \theta_{th}$), the phase shifts in the overcritical and critical regimes are in the range $(\frac{\pi}{2}, \pi)$, which means negative q in the framework of the initial Fano theory. In addition, the phase shift of $(-\pi, -\frac{\pi}{2}) \cup (\frac{\pi}{2}, \pi)$ in the undercritical regime represents both positive and negative q .

(iii) When the incident angle is closed to the mode angle ($\theta \rightarrow \theta_{th}$), in the framework of the initial Fano theory, the overcritical, critical, and undercritical regimes correspond to the symmetric valley, peak, and valley, respectively.

The phase shifts of the Fano interference versus the incident angle in different regimes are summarized in Table I. Summing up, in the framework of the initial Fano theory, the overcritical regime will show the asymmetric profile with positive q (left valley and right peak), and the symmetric valley and asymmetric profile with negative q (left peak and right valley). The critical regime will show the asymmetric profile with positive q (left valley and right peak), and the symmetric

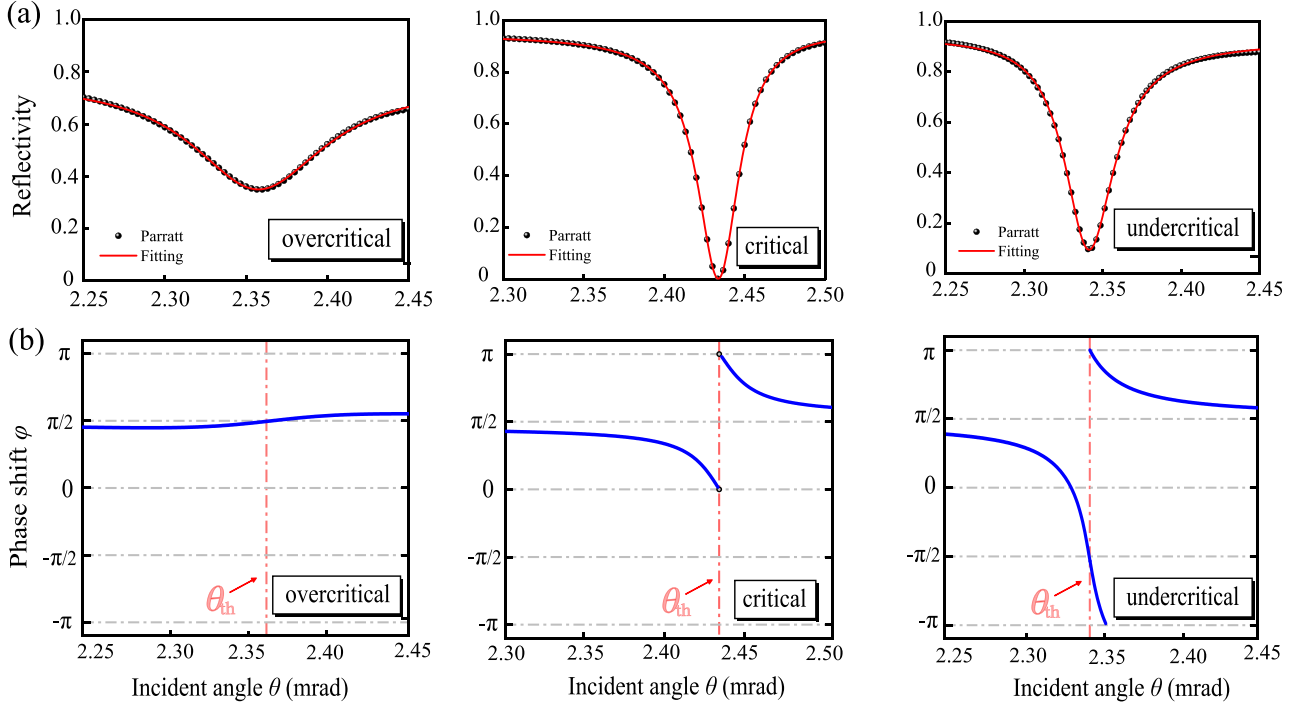


FIG. 2. (a) The reflectivities of different cavity regimes and fitted by the phenomenological model. (b) The phase shifts of the Fano interference versus the incident angle in different regimes.

peak and asymmetric profile with negative q (left peak and right valley). The undercritical regime will have more diverse asymmetric profiles in the thin-film planar cavity.

Replacing ^{56}Fe with ^{57}Fe (abundance = 100%), the spectra calculated by the CONUSS package [37,38] are shown in Fig. 3. Obviously, it can be seen that the asymmetry in the reflectivities shows a consistency in the angle offset regardless of the cavity regimes. Namely, the asymmetric profiles with positive q , symmetric Lorentz profile, and asymmetric profile with negative q are observed for the negative angle offset ($\Delta\theta < 0$), mode angle ($\Delta\theta = 0$), and positive angle offset ($\Delta\theta > 0$), respectively. It seems intuitively that there is a ‘‘contradiction’’ with the previous conclusions as mentioned above, especially the profiles in Figs. 3(c)–3(d), 3(f), and 3(i), i.e., there should be more variable asymmetric profiles in Figs. 3(c) and 3(i) and symmetric valley in Figs. 3(d) and 3(f).

For the Fano resonance, the general expression can be expressed as

$$\left| \frac{q + \varepsilon}{\varepsilon + i} \right|^2 = \left| 1 + \frac{q - i}{\varepsilon + i} \right|^2 = \left| 1 + \frac{|q - i|e^{-i\varphi}}{\varepsilon + i} \right|^2, \quad (5)$$

where the phase difference φ is the argument angle of the complex number $(q - i)$. The asymmetry of the Fano resonance

is mainly related to the sign of $\text{Re}(q - i)$, i.e., the positive $\text{Re}(q - i)$ has the right peak and left valley, and negative $\text{Re}(q - i)$ has the left peak and right valley. From the expression mentioned above, the sign of $\text{Re}(q - i)$ depends on the phase difference φ obviously. In detail, the sign of $\text{Re}(q - i)$ can be given by $|q - i| \cos \varphi$.

For the general case such as the results in Ref. [55] where q is a real number, $\text{Im}(q - i)$ always equals -1 . In this case, $\text{Re}(q - i)$ has a simpler expression of $q = \cot \varphi$, where not only the sign of $\text{Re}(q - i)$ but also its value can be given concurrently. In such a case, the phase range of φ is $(0, \pi)$ and it makes the same sign for $\cos \varphi$ and $\cot \varphi$.

Indeed, $q = \cot \varphi$ is valid only for the case where the asymmetric q is a real value in the initial situation of the Fano theory [44,45]. Recently, due to the broken time-reversal symmetry (TRS), the asymmetry q has been extended to the complex plane [56–61]. For the complex q number, $\text{Im}(q - i)$ can be any value, and the phase range of φ is not limited to $(0, \pi)$. In this case, the sign of the $\text{Re}(q - i)$ must be given by $|q - i| \cos \varphi$, and its value is not determined only by the phase difference. Therefore, it can be seen clearly that besides the phase range being expanded obviously for the complex q number, $q = \cot \varphi$ is only the special case for the real q number.

Combining Eqs. (2) and (5), the complex asymmetry q in the thin-film planar cavity reads

$$q = \frac{c}{r_c} \Pi e^{-i\varphi} + i, \quad (6)$$

where $\Pi = N\Gamma_s / (N\Gamma_s + \gamma)$ is the collective resonant strength (CRS) with values from 0 to 1. It can be seen that the value of q is directly connected with the CRS. In the presence of the complex q , the Fano resonance can be considered as an

TABLE I. Three cases of the phase shift in Fig. 2(b).

Incident angle	Phase range		
	Overcritical	Critical	Undercritical
$\theta < \theta_{th}$	$(0, \frac{\pi}{2})$	$(0, \frac{\pi}{2})$	$(-\frac{\pi}{2}, \frac{\pi}{2})$
$\theta = \theta_{th}$	$\frac{\pi}{2}$	$\frac{\pi}{2}$	$-\frac{\pi}{2}$
$\theta > \theta_{th}$	$(\frac{\pi}{2}, \pi)$	$(\frac{\pi}{2}, \pi)$	$(-\pi, -\frac{\pi}{2}) \cup (\frac{\pi}{2}, \pi)$

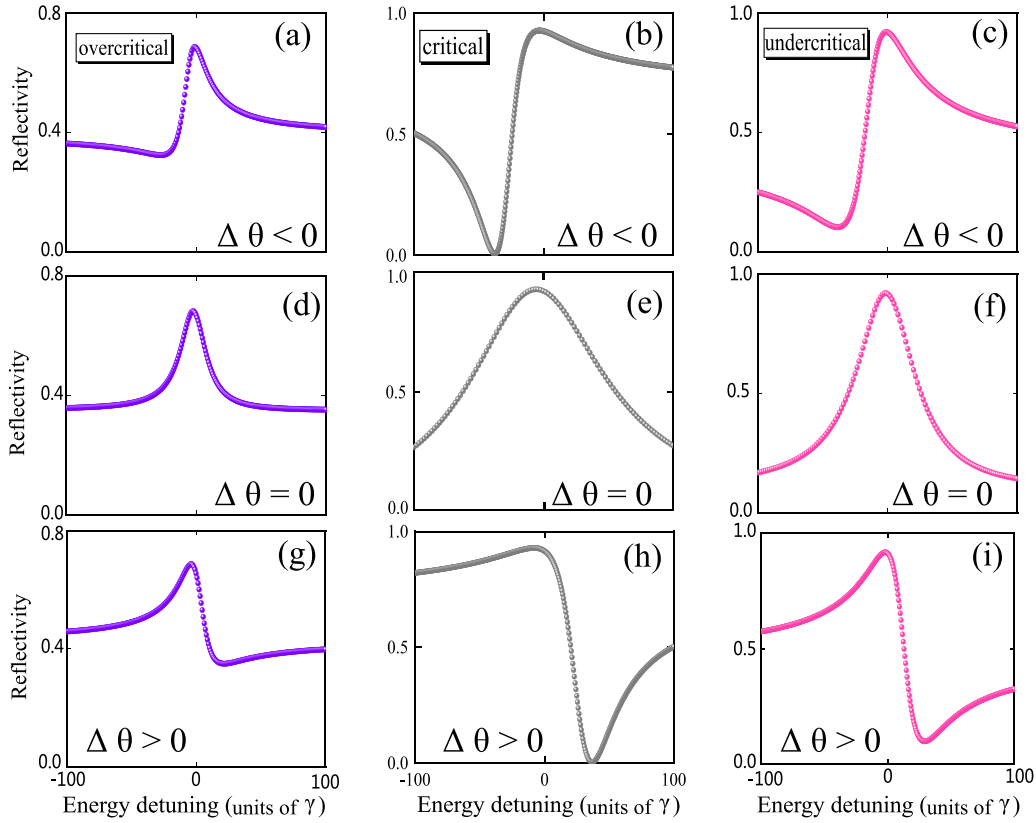


FIG. 3. The numerical reflectivities calculated by the benchmark CONUSS package [37,38] around the first cavity mode in different cavity regimes.

incoherent superposition between the normal Fano resonance and an extra Lorentz peak, viz. the Fano-Lorentz or Fano-Liouville shape [50,58,62]:

$$|R|^2 = \frac{[\text{Re}(q) + \varepsilon]^2}{\varepsilon^2 + 1} + \frac{[\text{Im}(q)]^2}{\varepsilon^2 + 1}. \quad (7)$$

Here, $\varepsilon = 2(\Delta - \Delta_{LS})/(N\Gamma_s + \gamma)$ is the dimensionless energy.

Remarkably, the extra Lorentz peak is symmetric, and its contribution to both sides of the Fano profile is symmetric, due to the incoherent superposition between the two sides of the Fano profile and the Lorentz peak. Hence, the asymmetry of the Fano-Lorentz profiles in the general case will not be changed, i.e., the asymmetric profile with positive q (left valley and right peak) will keep its asymmetric contour except for changing the height and width of the profile. In Figs. 3(c)–3(d), 3(f), and 3(i), however, the profiles are all changed according to the initial Fano theory. Frankly speaking, there are not symmetric valleys in Figs. 3(d) and 3(f) and are not more variable asymmetric profiles in Figs. 3(c) and 3(i).

In order to explain the contradiction as mentioned above, the initial Fano formula and Eq. (7) are compared. For the real q , the asymmetry of the profile depends on $\cot\varphi$. For the complex q , the asymmetry of the profile depends on the $\text{Re}(q)$, which is determined by the $\cos\varphi$. Hence, the dependence on phase difference of the asymmetry of the Fano profile is different for the real and complex q . In the critical regime, the complex q can be regarded as the real number owing to

$\text{Re}(q) \gg \text{Im}(q)$ [42,63]. In the overcritical and undercritical regimes, their real and imaginary components of q are comparable, so the Fano profiles influenced by $\text{Im}(q)$ can be studied in such cavity regimes.

B. Fano profiles influenced by $\text{Im}(q)$

In Eq. (2), the reflectivity of the symmetric peaks at the cavity mode angle can be simplified as

$$|R|^2 = \frac{(c-1)^2}{\eta} \left(\frac{\eta\varepsilon^2}{\varepsilon^2 + 1} + \frac{1-\eta}{\varepsilon^2 + 1} \right) \quad (8)$$

with

$$\eta = \frac{1}{1 + \left(1 - \frac{c}{c-1}\Pi\right)^2}. \quad (9)$$

Here η represents the weight of the normal Fano resonance in the Fano-Lorentz shape. Remarkably, it is the “window resonance” with $q = 0$ when $\eta = 1$, while a Lorentz peak when $\eta = 0$. In detail, the range of η depends on the cavity regimes (c) mainly viz.

$$\eta \in \left(0, \frac{1}{2}\right] \cup \left[\frac{1}{2}, \eta_{\max}\right], \text{ overcritical regime } (1 < c < 2);$$

$$\eta \in \left(0, \frac{1}{2}\right), \text{ undercritical regime } (0 < c < 1).$$

For the undercritical regime cavity where the total cavity decay rate is larger than the in- and outcoupling of light from the cavity, the contribution from the dissipation channel is larger than the resonant channel. Hence, $\eta < \frac{1}{2}$ always

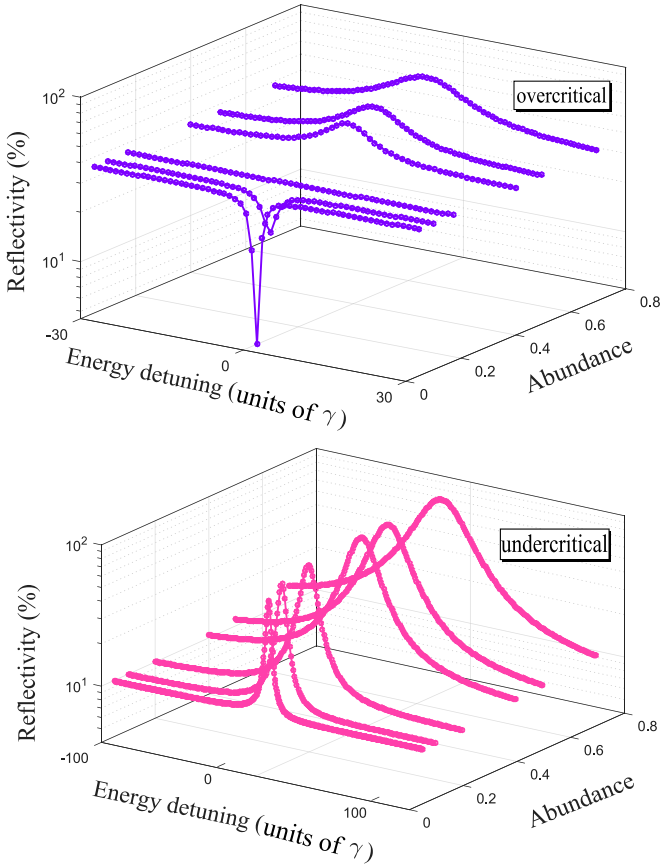


FIG. 4. The Fano-Lorentz shapes adjusted by the nuclear abundance in the overcritical and undercritical regimes.

means that the Lorentz peak is more significant than the window resonance. In this case, the symmetric valley will not be detected. On the contrary, for the overcritical regime cavity where the total cavity decay is less than the in- and outcoupling of light from the cavity, the contribution from the dissipation channel is weaker than the resonant channel. Hence, the Fano-Lorentz shape can show the symmetric valley or peak, and the transformation depends on the weight factor η . For a designed cavity, the weight η is only related to the CRS(Π) that can be adjusted by the nuclear abundance as mentioned above. To this end, the profiles at the mode angle with different nuclear abundances are calculated and shown in Fig. 4. In the overcritical regime, the resonant peaks weaken progressively and the symmetric valleys subsequently appear as the abundance decreases, whereas there are always resonant peaks in the undercritical regime.

More importantly, it should be noted that $\eta = \frac{1}{2}$, the same weight factor between the window resonance and extra Lorentz peak, is a critical case in the overcritical regime where the reflectivity is a constant that equals the value of the bare cavity, i.e., the resonant nuclear ensemble seems to be unexcited superficially. From Eq. (9), $\eta = \frac{1}{2}$ corresponds to a critical effective nuclear number N_c , which reads

$$N_c = \frac{2(c-1)\gamma}{2-c}\Gamma_s. \quad (10)$$

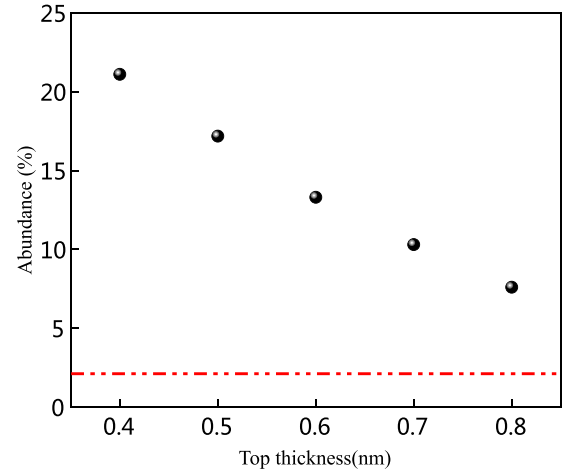


FIG. 5. The critical nuclear abundance in overcritical cavity with different top-layer thickness. The red line represents the natural abundance of ^{57}Fe .

It can be seen that the nonzero effective nuclear number requires the overcritical regime ($1 < c < 2$). It should be noted that the flat line is not a particular case, but a common phenomenon in the overcritical cavity regime, i.e., the critical nuclear abundance is different in different overcritical cavities. For the thin-film planar cavity, the valid condition of the overcritical cavity depends on the top mirror layer mainly, and the critical nuclear abundance is very sensitive to the top-layer thickness. In order to make it clear, several overcritical cavities with different top-layer thicknesses are designed. Considering the lattice parameter of Pt is 0.39 nm, the top thickness is adjusted from 0.4 nm to 0.8 nm in turn, and a series of critical nuclear abundances are obtained as shown in Fig. 5, assuming the nuclear layer thickness is 0.6 nm [9]. In Fig. 5, it can be seen that the critical abundance decreases obviously as the thickness of the top layer increases. In reality, the control of the nuclear abundance can increase the tolerance of the nuclear layer thickness, which is helpful to the sample preparation. On the other hand, manipulating the nuclear abundance in this work has the unique advantage to adjust the resonant channel without influencing the bare cavity characteristic, i.e., the resonant scattering amplitude is controlled individually. However, for the inner-shell system of Ref. [39], adjusting the top mirror layer means the cavity geometry is changed, where the cavity parameters and the resonant scattering amplitude cannot be controlled separately. It should be noted that transferring the experiment presented in Ref. [39] to the case of Mössbauer nuclei is challenging with the current third synchrotron radiation, due to the very low intensity of nuclear scattering signals from the low nuclear abundance and ultrathin layer. However, the forthcoming x-ray sources such as the high-repetition-rate XFELs and the fourth-generation diffraction-limited storage rings may provide this possibility.

In addition, the difference between the overcritical and undercritical cavities can also be understood from the perspective of destructive interference. At the cavity mode angle,

Eq. (2) can be simplified as

$$|R|^2 = \left| 1 \pm \Pi \frac{c}{|c-1|} \cdot \frac{i}{\varepsilon+i} \right|^2 (c-1)^2, \quad (11)$$

where “-” and “+” represent destructive interference and constructive interference for the overcritical and undercritical regime, respectively. It can be seen that the relative amplitude of the discrete state can be controlled by the CRS(Π). To this end, there are always symmetric peaks for the constructive interference in the undercritical regime, while there are three line shapes controlled by the nuclear abundance for the destructive interference in the overcritical regime. Moreover, the critical effective nuclear number N_c can also be understood as where the contribution of the nuclear ensemble is wiped out by their cross term. This flat line has recently been observed experimentally utilizing electronic transition [39], and the present work indicates that this specific phenomenon can only be observed in the overcritical cavity regime for the electronic transition in the atomic ensemble.

IV. CONCLUSION

In this paper, Fano interference controlled by the collective effect is studied by the thin-film planar cavity. With the resonant Mössbauer nuclei embedded in such a setup, the phase difference behaviors of the two pathways are different in various cavity regimes. By analyzing the phase difference and the asymmetric profiles in different cavity regimes, it is found that the asymmetric profiles in the overcritical and undercritical regimes can be considered as the Fano-Lorentz type, and the asymmetry of the profiles depends on the $\cos\varphi$ owing to the complex q . On the other hand, when the profile of the normal Fano resonance is symmetric ($q=0$ or $q \rightarrow \pm\infty$), the extra Lorentz peak will affect the normal Fano profile obviously. In the thin-film planar cavity, the weight factor η of the normal Fano resonance in the Fano-Lorentz profile is related to the cavity regime and the nuclear abundance. In the undercritical regime, $0 < \eta < 1/2$, whereas η can surpass $1/2$ in the overcritical regime. Hence, the undercritical cavity always has symmetric peaks versus the nuclear abundance, while the transformation between the symmetric valley and peak can be controlled by nuclear abundance in the overcritical regime. Additionally, there is a critical nuclear abundance in the overcritical regime where the reflectivity has a flat line and the nuclear resonance seems to be unexcited superficially. The flat line can be considered as an alternative line shape qualitatively in the complex q space, which is induced by the controllable relative amplitude of the discrete state in the frame of destructive interference. More recently, we note that the transformation between the symmetric valley and peak is also reported in the hybrid optomechanical system [64]. In addition, different decoherence processes in the open quantum system make the complex q show different trajectories.

TABLE II. The fitted parameters in different regimes.

	Overcritical	Critical	Undercritical
A	0.76	0.94	0.93
β	0.00	-0.04	0.05
θ_{1st} (mrad)	2.358	2.434	2.341
κ_R ($10^{-2}\omega_0$)	1.78	0.32	0.28
κ ($10^{-2}\omega_0$)	2.12	0.64	0.82
$c = 2\kappa_R/\kappa$	1.68	1	0.68

Specifically, the dissipation process causes the complex q to be linear, while the unitary dephasing process is circular [56]. Hence, the thin-film planar cavity would be one of the candidates to study the different decoherence processes via the complex q of Fano resonance.

ACKNOWLEDGMENT

This work is supported by the National Natural Science Foundation of China (Grants No. 12334010 and No. U1932207).

APPENDIX: FITTING PROCESS ABOUT THE REFLECTIVITY

The reflectivity of the thin-film planar cavity is calculated by CONUSS [37,38] using a Parratt-like method, and then fitted using a phenomenological model to obtain the cavity parameters. However, when fitting the reflectivity of the bare cavity, two additional effects from the top layer should be considered [34]. The absorption from the top layer can weaken the reflectivity intensity and introduce a tiny dispersion. To this end, the reflectivity of the bare cavity can be fitted as follows:

$$r_{cfit} = A \left(-e^{i\beta} + \frac{2\kappa_R}{\kappa + i\Delta_c} \right), \quad (A.1)$$

where A and β are used to consider the absorption effect and the dispersion, respectively. In the manuscript, the fitted cavity parameters such as cavity mode angle θ_{th} , coupling strength κ_R , and cavity decay rate κ are shown in Table II. The density and refractive index of the layer are the basic input parameters when calculating the reflectivity, which are listed in Table III. Here, n is the refractive index of the layer. As for ^{57}Fe , its refractive index is not a constant around the resonant energy, but it can be calculated by the nuclear scattering amplitude as shown in the Supplemental Material of Ref. [26].

TABLE III. The used parameters of layers.

	Density (g/cm^3)	$\text{Re}(n)$	$\text{Im}(n)$
Pt	21.45	1.71×10^{-5}	2.52×10^{-6}
Pd	12.02	1.03×10^{-5}	3.23×10^{-6}
C	2.26	2.26×10^{-6}	1.23×10^{-9}
^{56}Fe	7.8	7.26×10^{-6}	3.31×10^{-7}

[1] M. O. Scully, E. S. Fry, C. H. Raymond Ooi, and K. Wódkiewicz, Directed Spontaneous Emission from an

Extended Ensemble of N Atoms: Timing is Everything, *Phys. Rev. Lett.* **96**, 010501 (2006).

- [2] A. A. Svidzinsky, J. T. Chang, and M. O. Scully, Dynamical Evolution of Correlated Spontaneous Emission of a Single Photon from a Uniformly Excited Cloud of N Atoms, *Phys. Rev. Lett.* **100**, 160504 (2008).
- [3] T. Bienaimé, N. Piovella, and R. Kaiser, Controlled Dicke Subradiance from a Large Cloud of Two-Level Systems, *Phys. Rev. Lett.* **108**, 123602 (2012).
- [4] W. Guerin, M. O. Araújo, and R. Kaiser, Subradiance in a Large Cloud of Cold Atoms, *Phys. Rev. Lett.* **116**, 083601 (2016).
- [5] M. O. Scully, Collective Lamb Shift in Single Photon Dicke Superradiance, *Phys. Rev. Lett.* **102**, 143601 (2009).
- [6] J. Keaveney, A. Sargsyan, U. Krohn, I. G. Hughes, D. Sarkisyan, and C. S. Adams, Cooperative Lamb Shift in an Atomic Vapor Layer of Nanometer Thickness, *Phys. Rev. Lett.* **108**, 173601 (2012).
- [7] Z. Meir, O. Schwartz, E. Shahmoon, D. Oron, and R. Ozeri, Cooperative Lamb Shift in a Mesoscopic Atomic Array, *Phys. Rev. Lett.* **113**, 193002 (2014).
- [8] R. G. DeVoe and R. G. Brewer, Observation of Superradiant and Subradiant Spontaneous Emission of Two Trapped Ions, *Phys. Rev. Lett.* **76**, 2049 (1996).
- [9] R. Röhlsberger, K. Schlage, B. Sahoo, S. Couet, and R. Ruffer, Collective Lamb shift in single-photon superradiance, *Science* **328**, 1248 (2010).
- [10] R. Heidemann, U. Raitzsch, V. Bendkowsky, B. Butscher, R. Löw, L. Santos, and T. Pfau, Evidence for Coherent Collective Rydberg Excitation in the Strong Blockade Regime, *Phys. Rev. Lett.* **99**, 163601 (2007).
- [11] A. Gaëtan, Y. Miroshnychenko, T. Wilk, A. Chotia, M. Viteau, D. Comparat, P. Pillet, A. Browaeys, and P. Grangier, Observation of collective excitation of two individual atoms in the Rydberg blockade regime, *Nat. Phys.* **5**, 115 (2009).
- [12] E. Urban, T. A. Johnson, T. Henage, L. Isenhower, D. D. Yavuz, T. G. Walker, and M. Saffman, Observation of Rydberg blockade between two atoms, *Nat. Phys.* **5**, 110 (2009).
- [13] L. M. Duan, M. D. Lukin, J. I. Cirac, and P. Zoller, Long-distance quantum communication with atomic ensembles and linear optics, *Nature (London)* **414**, 413 (2001).
- [14] Y. Colombe, T. Steinmetz, G. Dubois, F. Linke, D. Hunger, and J. Reichel, Strong atom–field coupling for Bose–Einstein condensates in an optical cavity on a chip, *Nature (London)* **450**, 272 (2007).
- [15] Y. Kaluzny, P. Goy, M. Gross, J. M. Raimond, and S. Haroche, Observation of Self-Induced Rabi Oscillations in Two-Level Atoms Excited Inside a Resonant Cavity: The Ring Regime of Superradiance, *Phys. Rev. Lett.* **51**, 1175 (1983).
- [16] F. Rajabi and M. Houde, Dicke’s superradiance in astrophysics. I. The 21 cm line, *Astrophys. J.* **826**, 216 (2016).
- [17] R. Röhlsberger, K. Schlage, T. Klein, and O. Leupold, Accelerating the Spontaneous Emission of X Rays from Atoms in a Cavity, *Phys. Rev. Lett.* **95**, 097601 (2005).
- [18] J. Kim, D. Yang, S. Oh, and K. An, Coherent single-atom superradiance, *Science* **359**, 662 (2018).
- [19] R. Reimann, W. Alt, T. Kampschulte, T. Macha, L. Ratschbacher, N. Thau, S. Yoon, and D. Meschede, Cavity-Modified Collective Rayleigh Scattering of Two Atoms, *Phys. Rev. Lett.* **114**, 023601 (2015).
- [20] M. Scheibener, T. Schmidt, L. Worschech, A. Forchel, G. Bacher, T. Passow, and D. Hommel, Superradiance of quantum dots, *Nat. Phys.* **3**, 106 (2007).
- [21] S. Inouye, A. P. Chikkatur, D. M. Stamper-Kurn, J. Stenger, D. E. Pritchard, and W. Ketterle, Superradiant Rayleigh scattering from a Bose-Einstein condensate, *Science* **285**, 571 (1999).
- [22] B. W. Adams, C. Buth, S. M. Cavaletto, J. Evers, Z. Harman, C. H. Keitel, A. Pálffy, A. Picón, R. Röhlsberger, Y. Rostovtsev, and K. Tamasaku, X-ray quantum optics, *J. Mod. Opt.* **60**, 2 (2013).
- [23] A. Chumakov, A. Baron, I. Sergureev, C. Strohm, O. Leupold, Y. Shvydko, G. Smirnov, R. Ruffer, Y. Inyushin, M. Yabashi, K. Tono, T. Kudo, and T. Ishikawa, Superradiance of an ensemble of nuclei excited by a free electron laser, *Nat. Phys.* **14**, 261 (2018).
- [24] R. Schneider, T. Mehringer, G. Mercurio, L. Wenthaus, A. Classen, G. Brenner, O. Gorobtsov, A. Benz, D. Bhatti, L. Bocklage, B. Fischer, S. Lazarev, Y. Obukhov, K. Schlage, P. Skopintsev, J. Wagner, F. Waldmann, S. Willing, I. Zaluzhnyy, W. Wurth *et al.*, Quantum imaging with incoherently scattered light from a free-electron laser, *Nat. Phys.* **14**, 126 (2018).
- [25] J. Haber, J. Gollwitzer, S. Francoual, M. Tolkiehn, J. Stremfper, and R. Röhlsberger, Spectral Control of an X-Ray L-Edge Transition via a Thin-Film Cavity, *Phys. Rev. Lett.* **122**, 123608 (2019).
- [26] R. Röhlsberger, H. C. Wille, K. Schlage, and B. Sahoo, Electromagnetically induced transparency with resonant nuclei in a cavity, *Nature (London)* **482**, 199 (2012).
- [27] X. J. Kong and A. Pálffy, Stopping Narrow-Band X-Ray Pulses in Nuclear Media, *Phys. Rev. Lett.* **116**, 197402 (2016).
- [28] K. P. Heeg, H. C. Wille, K. Schlage, T. Guryeva, D. Schumacher, I. Uschmann, K. S. Schulze, B. Marx, T. Kämpfer, G. G. Paulus, R. Röhlsberger, and J. Evers, Vacuum-Assisted Generation and Control of Atomic Coherences at X-Ray Energies, *Phys. Rev. Lett.* **111**, 073601 (2013).
- [29] J. Harber, X. J. Kong, C. Strohm, S. Willing, J. Gollwitzer, L. Bocklage, R. Ruffer, A. Pálffy, and R. Röhlsberger, Rabi oscillations of X-ray radiation between two nuclear ensembles, *Nature Photon* **11**, 720 (2017).
- [30] X. C. Huang, X. J. Kong, T. J. Li, Z. R. Ma, H. C. Wang, G. C. Liu, Z. S. Wang, W. B. Li, and L. F. Zhu, Controlling core-hole lifetime through an x-ray planar cavity, *Phys. Rev. Res.* **3**, 033063 (2021).
- [31] L. G. Pattatt, Surface studied of solids by total reflection of x-rays, *Phys. Rev.* **95**, 359 (1954).
- [32] R. Röhlsberger, *Nuclear Condensed Matter Physics with Synchrotron Radiation: Basic Principles, Methodology and Applications* (Springer Science & Business Media, New York, 2005).
- [33] K. P. Heeg and J. Evers, X-ray quantum optics with Mössbauer nuclei embedded in thin-film cavities, *Phys. Rev. A* **88**, 043828 (2013).
- [34] K. P. Heeg and J. Evers, Collective effects between multiple nuclear ensembles in an X-ray cavity-QED setup, *Phys. Rev. A* **91**, 063803 (2015).
- [35] X. J. Kong, D. E. Chang, and A. Pálffy, Green’s-function formalism for resonant interaction of X rays with nuclei in structured media, *Phys. Rev. A* **102**, 033710 (2020).
- [36] D. Lentrod, K. P. Heeg, C. H. Keitel, and J. Evers, Ab initio quantum models for thin-film x-ray cavity QED, *Phys. Rev. Res.* **2**, 023396 (2020).
- [37] W. Sturhahn, CONUSS and PHOENIX: Evaluation of nuclear resonant scattering data, *Hyperfine Interact.* **125**, 149 (2000).

- [38] W. Sturhahn and E. Gerdau, Evaluation of time-differential measurements of nuclear-resonance scattering of x rays, *Phys. Rev. B* **49**, 9285 (1994).
- [39] Z. R. Ma, X. C. Huang, T. J. Li, H. C. Wang, G. C. Liu, Z. S. Wang, B. Li, W. B. Li, and L. F. Zhu, First Observation of New Flat Line Fano Profile via an X-Ray Planar Cavity, *Phys. Rev. Lett.* **129**, 213602 (2022).
- [40] J. Zhang, D. R. Lee, S. Narayanan, J. Wang, and S. K. Sinha, Waveguide-enhanced grazing-incidence small-angle x-ray scattering of buried nanostructures in thin films, *Phys. Rev. B* **84**, 075440 (2011).
- [41] O. Diekmann, D. Lentrodt, and J. Evers, Inverse design approach to x-ray quantum optics with Mössbauer nuclei in thin-film cavities, *Phys. Rev. A* **105**, 013715 (2022).
- [42] T. J. Li, X. C. Huang, Z. R. Ma, B. Li, and L. F. Zhu, Probing the dissipation process via a Fano resonance and collective effects in an X-ray cavity, *Phys. Rev. Res.* **4**, 023081 (2022).
- [43] J. Gollwitzer, L. Bocklage, R. Röhlberger, and G. Meier, Connecting Fano interference and the Jaynes-Cummings model in cavity magnonics, *NPJ Quantum Inf.* **7**, 114 (2021).
- [44] U. Fano, Effects of configuration interaction on intensities and phase shift, *Phys. Rev.* **124**, 1866 (1961).
- [45] K. Kobayashi, H. Aikawa, S. Katsumoto, and Y. Iye, Mesoscopic Fano effect in a quantum dot embedded in an Aharonov-Bohm ring, *Phys. Rev. B* **68**, 235304 (2003).
- [46] R. K. Adair, C. K. Bockelman, and R. E. Peterson, Experimental corroboration of the theory of neutron resonance scattering, *Phys. Rev.* **76**, 308 (1949).
- [47] F. Cerdeira, T. A. Fjeldly, and M. Cardona, Effect of free carriers on zone-center vibrational modes in heavily doped *p*-type Si. II. Optical modes, *Phys. Rev. B* **8**, 4734 (1973).
- [48] J. A. Armstrong and J. J. Wynne, Autoionizing States of Sr Studied by the Generation of Tunable Vacuum uv Radiation, *Phys. Rev. Lett.* **33**, 1183 (1974).
- [49] J. Göres, D. Goldhaber-Gordon, S. Heemeyer, M. A. Kastner, H. Shtrikman, D. Mahalu, and U. Meirav, Fano resonances in electronic transport through a single-electron transistor, *Phys. Rev. B* **62**, 2188 (2000).
- [50] K. Kobayashi, H. Aikawa, S. Katsumoto, and Y. Iye, Tuning of the Fano Effect through a Quantum Dot in an Aharonov-Bohm Interferometer, *Phys. Rev. Lett.* **88**, 256806 (2002).
- [51] X. J. Liu, L. F. Zhu, Z. S. Yuan, W. B. Li, H. D. Cheng, Y. P. Huang, Z. P. Zhong, K. Z. Xun, and J. M. Li, Dynamical Correlation in Double Excitations of Helium Studied by High-Resolution and Angular-Resolved Fast-Electron Energy-Loss Spectroscopy in Absolute Measurements, *Phys. Rev. Lett.* **91**, 193203 (2003).
- [52] A. E. Miroshnichenko, S. Flach, and Y. S. Kivshar, Fano resonances in nanoscale structures, *Rev. Mod. Phys.* **82**, 2257 (2010).
- [53] J. P. Connerade and A. M. Lane, Interacting resonances in atomic spectroscopy, *Rep. Prog. Phys.* **51**, 1439 (1988).
- [54] C. Ott, A. Kaldun, P. Raith, K. Meyer, M. Laux, J. Evers, C. H. Keitel, C. H. Greene, and T. Pfeifer, Lorentz meets Fano in spectral line shapes: A universal phase and its laser control, *Science* **340**, 716 (2013).
- [55] M. F. Limonov, M. V. Rybin, A. N. Poddubny, and Y. S. Kivshar, Fano resonances in photonics, *Nat. Photon.* **11**, 543 (2017).
- [56] A. A. Clerk, X. Waintal, and P. W. Brouwer, Fano Resonances as a Probe of Phase Coherence in Quantum Dots, *Phys. Rev. Lett.* **86**, 4636 (2001).
- [57] I. Avrutsky, R. Gibson, J. Sears, G. Khitrova, H. M. Gibbs, and J. Hendrickson, Linear systems approach to describing and classifying Fano resonances, *Phys. Rev. B* **87**, 125118 (2013).
- [58] D. Finkelstein-Shapiro, I. Urdaneta, M. Calatayud, O. Atabek, V. Mujica, and A. Keller, Fano-Liouville Spectral Signatures in Open Quantum Systems, *Phys. Rev. Lett.* **115**, 113006 (2015).
- [59] A. N. Poddubny, M. V. Rybin, M. F. Limonov, and Y. S. Kivshar, Fano interference governs wave transport in disordered systems, *Nat. Commun.* **3**, 914 (2012).
- [60] A. Bärthaler, S. Rotter, F. Libisch, and J. Burgdörfer, S. Gehler, U. Kuhl, and H. J. Stockmann, Probing Decoherence through Fano Resonances, *Phys. Rev. Lett.* **105**, 056801 (2010).
- [61] S. Rotter, F. Libisch, J. Burgdörfer, U. Kuhl, and H. J. Stockmann, Tunable Fano resonances in transport through microwave billiards, *Phys. Rev. E* **69**, 046208 (2004).
- [62] M. V. Rybin, P. V. Kapitanova, D. S. Filonov, A. P. Slobozhanyuk, P. A. Belov, Y. S. Kivshar, and M. F. Limonov, Fano resonances in antennas: General control over radiation patterns, *Phys. Rev. B* **88**, 205106 (2013).
- [63] K. P. Heeg, C. Ott, D. Schumacher, H. C. Wille, R. Röhlberger, T. Pfeifer, and J. Evers, Interferometric Phase Detection at X-ray Energies Via Fano Resonance Control, *Phys. Rev. Lett.* **114**, 207401 (2015).
- [64] Z. Shen, Y. L. Zhang, C. L. Zou, G. C. Guo, and C. H. Dong, Dissipatively Controlled Optomechanical Interaction via Cascaded Photon-Phonon Coupling, *Phys. Rev. Lett.* **126**, 163604 (2021).